

# Beyond Ground-Truth: Leveraging Image Quality Priors for Real-World Image Restoration

Fengyang Xiao<sup>1,\*</sup>, Peng Hu<sup>2,\*</sup>, Lei Xu<sup>3</sup>, XingE Guo<sup>1</sup>, Guanyi Qin<sup>1</sup>, Yuqi Shen<sup>2</sup>,  
Chengyu Fang<sup>2</sup>, Rihan Zhang<sup>1</sup>, Chunming He<sup>1,†</sup>, and Sina Farsiu<sup>1</sup>

<sup>1</sup>Duke University, <sup>2</sup>Tsinghua University, <sup>3</sup>EPFL

\* Equal Contribution, † Corresponding Author,

Contact: fengyang.xiao@duke.edu / tommypinkman47@gmail.com / chunming.he@duke.edu

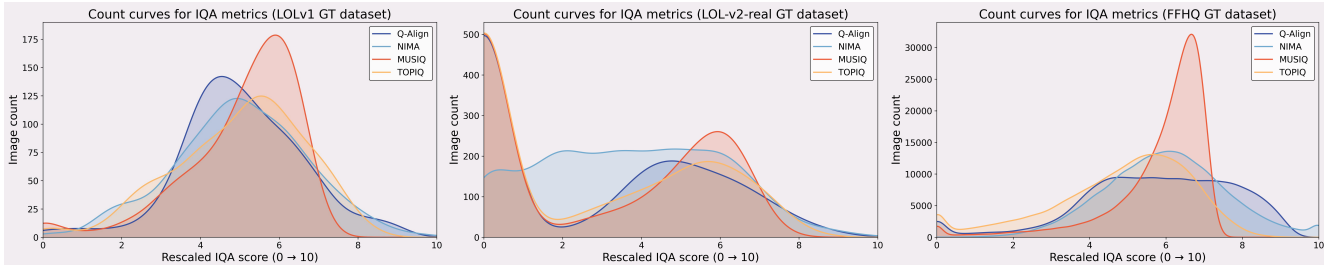


Figure 1. Score distributions given by different Image Quality Assessment (IQA) models across various ground truth datasets, where higher scores indicate better image quality. Notably, most ground-truth images exhibit an average quality score between 5 and 8, with some residual degradation patterns. This limits the network’s ability to output truly high-quality images, achieving scores closer to 9.

## Abstract

Real-world image restoration aims to restore high-quality (HQ) images from degraded low-quality (LQ) inputs captured under uncontrolled conditions. Existing methods typically depend on ground-truth (GT) supervision, assuming that GT provides perfect reference quality. However, GT can still contain images with inconsistent perceptual fidelity, causing models to converge to the average quality level of the training data rather than achieving the highest perceptual quality attainable. To address these problems, we propose a novel framework, termed **IQPIR**, that introduces an Image Quality Prior (IQP)—extracted from pre-trained No-Reference Image Quality Assessment (NR-IQA) models—to guide the restoration process toward perceptually optimal outputs explicitly. Our approach synergistically integrates IQP with a learned codebook prior through three key mechanisms: (1) a **quality-conditioned Transformer**, where NR-IQA-derived scores serve as conditioning signals to steer the predicted representation toward maximal perceptual quality. This design provides a plug-and-play enhancement compatible with existing restoration architectures without structural modification; and (2) a **dual-branch codebook structure**, which disentangles common and HQ-specific features, ensuring a comprehensive representation of both generic structural information and quality-sensitive attributes; and (3) a **discrete**

**representation-based quality optimization strategy**, which mitigates over-optimization effects commonly observed in continuous latent spaces. Extensive experiments on real-world image restoration demonstrate that our method not only surpasses cutting-edge methods but also serves as a generalizable quality-guided enhancement strategy for existing methods. The code is available at <https://github.com/fengyang1399-pixel/IQPIR>.

## 1. Introduction

Image restoration aims to reconstruct degraded low-quality (LQ) images into high-quality (HQ) outputs, yet real-world degradations are complex and unknown, making the task highly ill-posed. Recent works leverage diverse priors to enrich details and enhance robustness under various degradations[30, 31, 36, 47, 49, 63]. Among them, codebook-based methods[10, 45, 48, 66] formulate restoration as a code prediction problem in a discrete representation space, effectively reducing reconstruction ambiguity and improving resilience to degradation diversity.

However, a basic limitation of existing methods lies in the implicit assumption that high-quality ground truth (GT) data are flawless and should serve as the sole supervision source. As shown in Fig. 1, the perceptual quality within these GT datasets is often inconsistent and suboptimal. Consequently, most models restore LQ inputs only

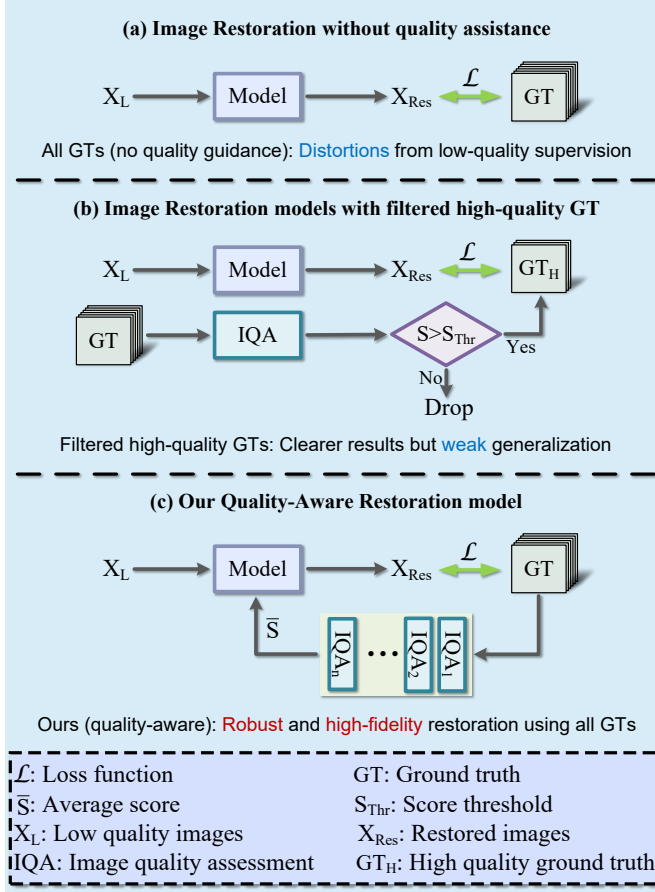


Figure 2. Structural comparison of different training paradigms, where both (b) and our (c) utilize IQA to guide network training.

to match the average GT quality, rather than pursuing the highest achievable perceptual fidelity. Although employing NR-IQA models to filter out and retain only the highest-quality (HQ+) images can improve overall output quality, this strategy inevitably reduces data diversity, as top-tier GT samples constitute only a small subset, as shown in Fig. 2. Over-reliance on such curated data may lead to artifacts and degraded feature representations in the restored outputs.

To overcome this, we propose a novel framework that uses an Image Quality Prior to address the suboptimal restoration quality caused by imperfect GT. Our IQP is derived from pre-trained Non-Reference Image Quality Assessment (NR-IQA) models, which enables our restoration model to distinguish between different quality levels and associate images with their corresponding quality scores. Instead of blindly pursuing a match to imperfect GT, our core idea is to explicitly guide the restoration process toward the highest possible perceptual quality. As shown in Fig. 3, our strategy can also facilitate cutting-edge methods.

We introduce a novel framework, IQPIR, that seamlessly integrates image quality and codebook priors to enhance restoration quality. We first obtain an image quality prior from NR-IQA models and incorporate it at different train-

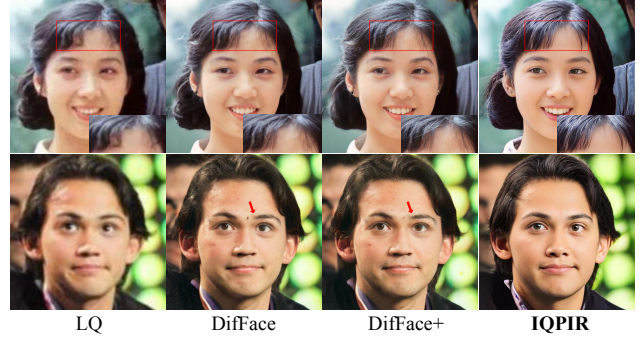


Figure 3. Results on blind face restoration. DiffFace+ is the DiffFace [58] with our quality prior conditioned approach, having more details. Our IQPIR has the highest perceptual quality.

ing stages. In the code prediction stage, we use a **quality-conditioned Transformer** that takes the quality score as a condition during code prediction. This allows the model to generate images with the highest quality when provided with the highest score as a condition. The feasibility of this score-conditioned manner stems from the inconsistent quality of training data, making it applicable to other restoration models. We also leverage the discrete representation space of the codebook for quality optimization, which mitigates the over-optimization issue common in continuous representations. Furthermore, different GT quality tiers offer distinct functional advantages: High-Quality (HQ) GT excels in controlling fine-grained structures (e.g., hair-end details), while average GT is more effective for generalized recovery from casual, large-area distortions (e.g., blurs). Based on this principle, in the codebook prior learning stage, we introduce a **dual-codebook architecture**, comprising a common codebook and an HQ+ codebook, to learn both general and high-quality-specific features. Together, these innovations enable robust and perceptually consistent restoration across diverse real-world conditions.

In summary, our main contributions are as follows:

- (1) We propose a novel prior-based method, IQPIR, which uses an image quality prior to help restoration models understand HQ features and improves the ability to generate HQ results. This bridges the gap between an image quality prior and its application in enhancing restoration quality.
- (2) We introduce a series of strategies for integrating image quality prior with codebook prior, including a plug-and-play score-conditioned approach, a quality optimization technique based on discrete representation, and a dual-codebook reconstruction model. These strategies leverage the advantages of the image quality prior across multiple stages to enhance restoration quality.
- (3) Experiments demonstrate that IQPIR effectively generalizes across various real-world restoration tasks, consistently delivering superior perceptual quality and robustness compared to existing state-of-the-art methods.

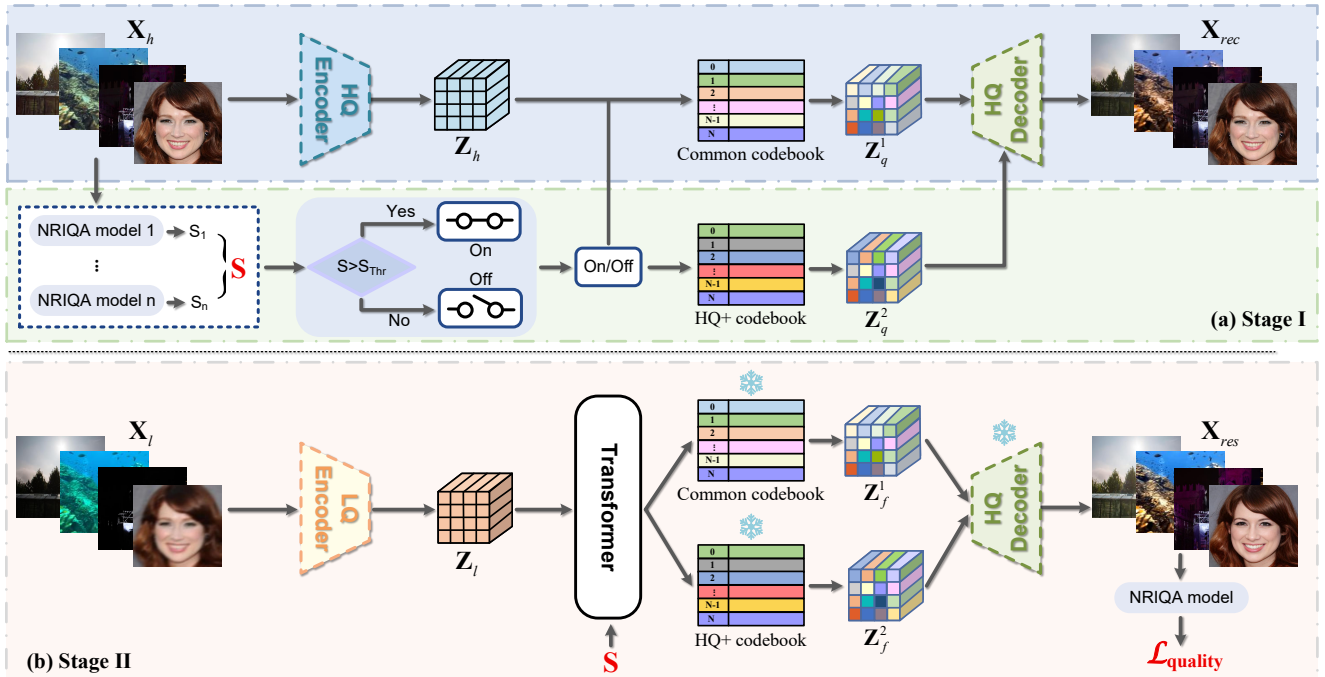


Figure 4. **Overall framework of IQPIR.** (a) In the codebook learning stage, a dual-codebook architecture is proposed. The HQ+ codebook is learned to quantize  $Z_h$  only when the quality score of  $x_h$  is higher than the threshold  $S_{thr}$ . (b) In the codebook lookup stage, we input the quality score  $S$  as a condition into Transformer  $T$ , which predicts two code sequences at the same time. The two codebooks are leveraged to look up the corresponding code entries. Finally, the NR-IQA model is utilized to calculate the quality loss  $\mathcal{L}_{quality}$ .

## 2. Related Work

**Real-world image restoration.** RWIR aims to recover HQ images from degraded LQ inputs affected by authentic noise, blur, or illumination variations [5, 15, 16, 19, 43]. Early works relied on explicit degradation modeling [15] or paired data synthesis [59], but limited by inaccurate assumptions. Later approaches leveraged large-scale datasets [57] or degradation-aware architectures [14] to better approximate real-world conditions. Recent methods, such as domain adaptation [7], unpaired learning [13], and self-supervised objectives [18], further reduce the gap between synthetic and real data. However, most methods still assume that GT images are perfect, even though datasets like FFHQ [25] exhibit uneven perceptual quality, leading models to converge toward average GT fidelity rather than optimal perceptual quality. Our IQPIR introduces an image quality prior derived from NR-IQA models to guide training toward higher-quality reconstructions under diverse degradations.

**Prior-based image restoration.** Priors play a crucial role in restoration problems. Common priors include geometric [22, 36], reference [29–31], generative [17, 20, 47, 49, 63], and codebook priors [10, 45, 66]. Geometric priors provide structural cues [2, 22] but degrade under heavy distortions. Reference priors [30, 33] rely on extra HQ data, limiting applicability. Generative priors [28, 49, 63] exploit pretrained models for semantic completion but may hallucinate. Codebook priors [10, 45, 66], based on vector quan-

tization [6], stabilize restoration by learning discrete representations, achieving perceptual gains. Yet, they assume flawless GT supervision, overlooking quality inconsistency within training data. Our IQPIR extends codebook-based methods with an image quality prior as a perception-aware constraint, enabling the network to adaptively emphasize high-quality cues and achieve high-fidelity restoration.

## 3. Methodology

To address the challenge of real-world image restoration (RWIR), where degradations are complex and annotations imperfect, we introduce IQPIR, a unified framework that incorporates Image Quality Priors (IQPs) into both the codebook learning and code prediction stages. The pipeline is shown in Fig. 4. IQPIR integrates perceptual quality awareness into the discrete representation learning process to produce outputs of the highest attainable fidelity and realism.

In the first stage, a dual-codebook architecture is trained to disentangle universal structural features from high-quality (HQ+) attributes (Sec. 3.1). In the second stage, a quality-prior-conditioned transformer exploits the learned dual codebook for restoration, with image quality priors integrated both as input conditions and as optimization objectives (Secs. 3.2 and 3.3).

### 3.1. Dual Codebook Learning

Real-world images exhibit highly variable perceptual quality. To robustly represent both common structures and high-

quality details, we employ a dual codebook design with a common codebook and a high-quality (HQ+) codebook.

During training, HQ images  $x_h$  are first encoded by the feature extractor  $E$  and quantized via the common codebook to obtain  $Z_q^1$ . If a given image’s quality score  $S$ , estimated using a No-Reference Image Quality Assessment (NR-IQA) model, exceeds a threshold  $S_{thr}$ , its features are further quantized using the HQ+ codebook to generate  $Z_q^2$ . The final quantized feature is defined as

$$Z_q = \begin{cases} Z_q^1 + \alpha Z_q^2 & \text{if } S > S_{thr}, \\ Z_q^1 & \text{if } S \leq S_{thr}. \end{cases} \quad (1)$$

where  $\alpha$  balances the contributions of the two codebooks. The decoder  $D$  then reconstructs the image  $x_{rec}$  from  $Z_q$ .

The common codebook learns generic structures across diverse training data, while the HQ+ codebook specializes in the fine-grained visual details of high-quality samples. This separation enables the model to preserve general fidelity while enhancing perceptual quality. At inference, both codebooks are jointly leveraged, allowing the model to synthesize HQ+ outputs even from degraded inputs.

### 3.2. Quality Prior Condition

Before training, we first employ NR-IQA models to assess the quality score of GT data, denoted as  $S$ . In the codebook lookup stage, we introduce the quality prior as an additional condition for code prediction using a conditional Transformer. This Transformer model predicts two code sequences conditioned on the image quality score  $S$ . The conditional Transformer is trained to capture the relationship between GT images and their associated quality scores. Specifically, during training, when the highest quality score is used as the condition, the ground truth is set to the highest quality image. This strategy resembles class-conditional generation, enabling the model to learn quality-specific generation capabilities across diverse levels.

First, we extract the LQ feature via  $Z_l = E(x_l)$ . Then we embed the quality score  $S$  into an embedding vector  $\mathbf{s} \in \mathbb{R}^{h*w*c}$  and reshape it to  $\mathbf{s} \in \mathbb{R}^{h*w*c}$ , which matches the dimensionality of  $Z_l$ . This embedding vector  $\mathbf{s}$  is directly added to  $Z_l$ , formulated as:

$$\hat{Z}_l = Z_l + \mathbf{s}. \quad (2)$$

Upon receiving  $\hat{Z}_l$  as input, the Transformer  $T$  predicts two code sequences,  $\mathbf{c}_1$  and  $\mathbf{c}_2$ . Then  $\mathbf{c}_1$  retrieves code entries from the common codebook to construct the quantized feature  $Z_f^1$ , while  $\mathbf{c}_2$  retrieves code entries from the HQ+ codebook to form  $Z_f^2$ . We then fuse  $Z_f^1$  and  $Z_f^2$  to get  $Z_f$  via:

$$Z_f = Z_f^1 + \alpha Z_f^2, \quad (3)$$

where  $\alpha$  is the balance weight.  $Z_f$  is fed to the decoder to generate restoration images  $x_{res}$ . Since  $D$  is trained to reconstruct high-quality (HQ+) images from the fused representations  $Z_q^1$  and  $Z_q^2$ , it is capable of generating restora-

tions with comparable perceptual fidelity when taking the fused feature  $Z_f$  as input during the second stage.

By conditioning on the perceptual score  $S$ , the model learns the correspondence between input features and quality levels. During inference, setting  $S$  to its maximum value allows the network to produce restorations of the highest feasible perceptual fidelity, effectively achieving controllable quality restoration under real-world degradations.

**Quality Prior Ensembles.** Although existing NR-IQA methods are powerful, they may still harbor certain biases. To mitigate the impact of biases introduced by a single IQA model, we propose incorporating multiple IQA models as the final IQA prior. Specifically, we calculate the mean score of different IQA models:

$$S = \frac{1}{n} \sum_{i=1}^n s_i, \quad (4)$$

where  $s_i$  is the normalized score of the  $i$ -th IQA model. This ensemble method is used in both the codebook learning stage and the code prediction stage.

### 3.3. Quality Optimization

Using NR-IQA measures as objectives in image processing systems represents a promising but underexplored area. However, the optimization direction of NR-IQA objectives is unstable due to the absence of a reference. This can lead to the generation of images with low perceptual quality (or known as unrealistic) from a human perspective, known as **adversarial examples**, that nonetheless deceive NR-IQA models into assigning high scores. This phenomenon is known as over-optimization, a problem also observed in large-scale reward learning systems [9].

The presence of adversarial examples renders NR-IQA objectives unreliable. A fundamental solution involves reducing the presence of these examples within the output space. We demonstrate that a discrete codebook prior naturally supports this by restricting the output space to a finite set, significantly reducing the number of adversarial examples. Training the codebook on HQ images ensures that most samples within this finite space possess high-quality semantic information, further limiting adversarial examples. Thus, NR-IQA measures are well-suited as objectives for discrete codebook-based network structures. Based on this, we propose to maximize NR-IQA scores directly to fine-tune our model’s parameters.

**Final training objective.** In the second stage, three losses are utilized to train the encoder  $E$  and the transformer  $T$ :

$$\mathcal{L}_{feat} = \|Z_l - sg(Z_q)\|_2^2, \quad (5)$$

$$\mathcal{L}_{index} = \sum_{i=0}^{h*w-1} -\mathbf{c}_1^i \log(\hat{\mathbf{c}}_1^i) + \sum_{i=0}^{h*w-1} -\mathbf{c}_2^i \log(\hat{\mathbf{c}}_2^i), \quad (6)$$

$$\mathcal{L}_{quality} = -IQA(x_{res}), \quad (7)$$

Table 1. Results on blind face restoration. The best two results are in **red** and **blue** fonts, respectively.

Data.	Methods	TOPIQ-G $\uparrow$	Musiq-G $\uparrow$	Musiq-K $\uparrow$	Musiq-A $\uparrow$	Arniqa $\uparrow$	MDFS $\downarrow$	Q-Align $\uparrow$	CLIP-IQA $\uparrow$
LFW-Test	RestoreFormer[48]	0.793	0.807	73.70	4.65	0.711	18.64	4.22	0.741
	DR2[49]	0.720	0.753	67.13	4.67	0.700	18.43	4.23	0.658
	CodeFormer[66]	0.809	0.832	75.47	4.76	0.726	18.46	4.31	0.697
	DifFace[58]	0.718	0.748	69.90	4.48	0.686	18.41	3.86	0.610
	DAEFR[45]	0.814	0.827	75.84	4.81	0.742	<b>17.91</b>	4.33	0.696
	WaveFace[38]	0.786	0.799	73.55	4.69	0.689	19.18	4.43	<b>0.788</b>
	Interlcm[28]	<b>0.831</b>	<b>0.834</b>	<b>75.87</b>	<b>4.84</b>	<b>0.753</b>	17.98	<b>4.55</b>	0.721
	IQPIR (Ours)	<b>0.861</b>	<b>0.878</b>	<b>76.89</b>	<b>5.08</b>	<b>0.761</b>	<b>17.82</b>	<b>4.67</b>	<b>0.790</b>
WebPhoto-Test	RestoreFormer[48]	0.706	0.721	69.83	4.55	0.677	19.21	3.52	0.711
	DR2[49]	0.621	0.630	61.28	<b>4.88</b>	0.601	20.51	2.87	0.447
	CodeFormer[66]	0.756	0.782	73.56	4.69	0.687	19.10	3.84	0.691
	DifFace[58]	0.638	0.670	65.77	4.44	0.642	19.36	3.31	0.586
	DAEFR[45]	0.746	0.753	72.70	4.58	0.701	18.63	3.82	0.669
	WaveFace[38]	0.694	0.704	70.46	4.48	0.686	19.66	3.76	<b>0.778</b>
	Interlcm[28]	<b>0.794</b>	<b>0.807</b>	<b>75.82</b>	4.81	<b>0.731</b>	<b>18.45</b>	<b>3.99</b>	0.752
	IQPIR (Ours)	<b>0.822</b>	<b>0.849</b>	<b>76.86</b>	<b>4.96</b>	<b>0.742</b>	<b>18.30</b>	<b>4.23</b>	<b>0.783</b>
WIDER-Test	RestoreFormer[48]	0.714	0.733	67.83	4.49	0.691	19.04	3.55	0.727
	DR2[49]	0.731	0.758	67.76	4.73	0.601	20.06	2.87	0.523
	CodeFormer[66]	0.772	0.810	72.97	4.57	0.705	18.67	4.05	0.697
	DifFace[58]	0.684	0.715	65.04	4.36	0.644	18.88	3.60	0.597
	DAEFR[45]	0.787	0.807	74.15	4.60	0.721	<b>18.18</b>	4.17	0.697
	WaveFace[38]	0.751	0.778	72.90	4.70	0.686	19.81	4.12	<b>0.781</b>
	Interlcm[28]	<b>0.798</b>	<b>0.820</b>	<b>75.34</b>	<b>4.80</b>	<b>0.743</b>	18.26	<b>4.24</b>	0.754
	IQPIR (Ours)	<b>0.837</b>	<b>0.872</b>	<b>76.38</b>	<b>4.93</b>	<b>0.748</b>	<b>18.06</b>	<b>4.56</b>	<b>0.785</b>

where  $\mathcal{L}_{feat}$  denotes mean square error,  $\mathcal{L}_{index}$  is a cross-entropy loss, and  $\mathcal{L}_{quality}$  is a quality loss.  $sg(\cdot)$  denotes the stop-gradient operation.  $\mathcal{L}_{index}$  takes the HQ code indices  $\mathbf{c}_1$  and  $\mathbf{c}_2$  from the two codebooks as supervision targets, guiding  $T$  to predict the corresponding indices and thereby reconstruct the correct HQ representations during decoding. For  $\mathcal{L}_{feat}$ , the ground-truth  $Z_q$  is obtained via:

$$Z_q = Z_q^1 + \alpha Z_q^2, \quad (8)$$

where  $Z_q^1$  and  $Z_q^2$  are retrieved from the two codebooks according to the predicted indices  $\mathbf{c}_1$  and  $\mathbf{c}_2$ .  $Z_q$  is computed following the same manner in Eq. (1) when  $S > S_{thr}$  (i.e., for HQ+ images). Consequently, the feature reconstruction loss  $\mathcal{L}_{feat}$  guides the network to align the LQ feature representation with its corresponding HQ+ counterpart.

Leveraging the inherent constraint of the discrete codebook prior, which restricts the output space and mitigates the generation of adversarial artifacts, we further introduce a perceptual enhancement term based on NR-IQA scores. This perception-based objective is formulated as:

$$\mathcal{L}_{quality} = -IQA(x_{res}), \quad (9)$$

which encourages the model to progressively refine perceptual quality throughout optimization.

The final training objective is therefore expressed as:

$$\mathcal{L}_f = \mathcal{L}_{feat} + \lambda_1 \mathcal{L}_{index} + \lambda_2 \mathcal{L}_{quality}, \quad (10)$$

where  $\lambda_1$  and  $\lambda_2$  are set to 0.5 and 0.1, respectively. This formulation enables IQPIR to balance reconstruction accu-

racy and perceptual refinement by directly aligning optimization with perceptual quality metrics.

## 4. Experiments

**Implementation Details.** IQPIR is implemented in PyTorch and trained on one NVIDIA H200 GPU. The quantized feature maps have dimensions of  $16 \times 16 \times 256$ , and each codebook consists of 1024 entries, each with a 256-dimensional embedding. We adopt Adam with momentum terms of (0.9,0.999) and set the batch size to 32.

For our quality priors, we employ an ensemble of three advanced NR-IQA models, incorporating traditional and MLLM-based methods to estimate the final quality score. For the face task, this ensemble specifically integrates two traditional approaches (Musiq-GFIQA and TOPIQ-GFIQA, both trained on GFIQA[44]) with one MLLM-based method (Q-Align [51]). In other tasks, quality assessment is performed using Musiq[26], CLIP-IQA[46], and BRISQUE[39].

### 4.1. Comparative Evaluation

**Blind face restoration.** Following the common setting [58, 66], we train our model on *FFHQ* and evaluate the performance on three real-world data: LFW-Test [23], WebPhoto-Test [47], and WIDER-Test [66]. We apply 8 NR-IQA metrics for evaluation, including Musiq-Koniq [26], Musiq-GFIQA [26], and TOPIQ-GFIQA [3], Musiq-AVA [26] (for

Table 2. Results on low-light image enhancement.

Methods	Sources	<i>LOL-v1</i>				<i>LOL-v2-real</i>				<i>LOL-v2-synthetic</i>			
		PSNR $\uparrow$	SSIM $\uparrow$	FID $\downarrow$	BIQE $\downarrow$	PSNR $\uparrow$	SSIM $\uparrow$	FID $\downarrow$	BIQE $\downarrow$	PSNR $\uparrow$	SSIM $\uparrow$	FID $\downarrow$	BIQE $\downarrow$
CUE [64]	ICCV23	21.86	0.841	69.83	27.15	21.19	0.829	67.05	28.83	24.41	0.917	31.33	33.83
GSAD [24]	NIPS23	23.23	0.852	51.64	19.96	20.19	0.847	46.77	28.85	24.22	0.927	19.24	25.76
AST [67]	CVPR24	21.09	0.858	87.67	21.23	21.68	0.856	91.81	25.17	22.25	0.927	37.19	28.78
MambaIR [12]	ECCV24	22.23	0.863	63.39	20.17	21.15	0.857	56.09	24.46	25.75	0.937	19.75	20.37
Reti-Diff [15]	ICLR25	<b>25.35</b>	0.866	49.14	17.75	22.97	0.858	<b>43.18</b>	23.66	<b>27.53</b>	<b>0.951</b>	<b>13.26</b>	<b>15.77</b>
CIDNet [54]	CVPR25	23.50	<b>0.900</b>	<b>46.69</b>	<b>14.77</b>	<b>24.11</b>	<b>0.871</b>	48.04	<b>18.45</b>	25.71	0.942	18.60	15.87
IQPIR	Ours	<b>25.72</b>	<b>0.902</b>	<b>40.18</b>	<b>13.32</b>	<b>24.20</b>	<b>0.889</b>	<b>40.05</b>	<b>13.39</b>	<b>27.60</b>	<b>0.953</b>	<b>12.04</b>	<b>15.30</b>

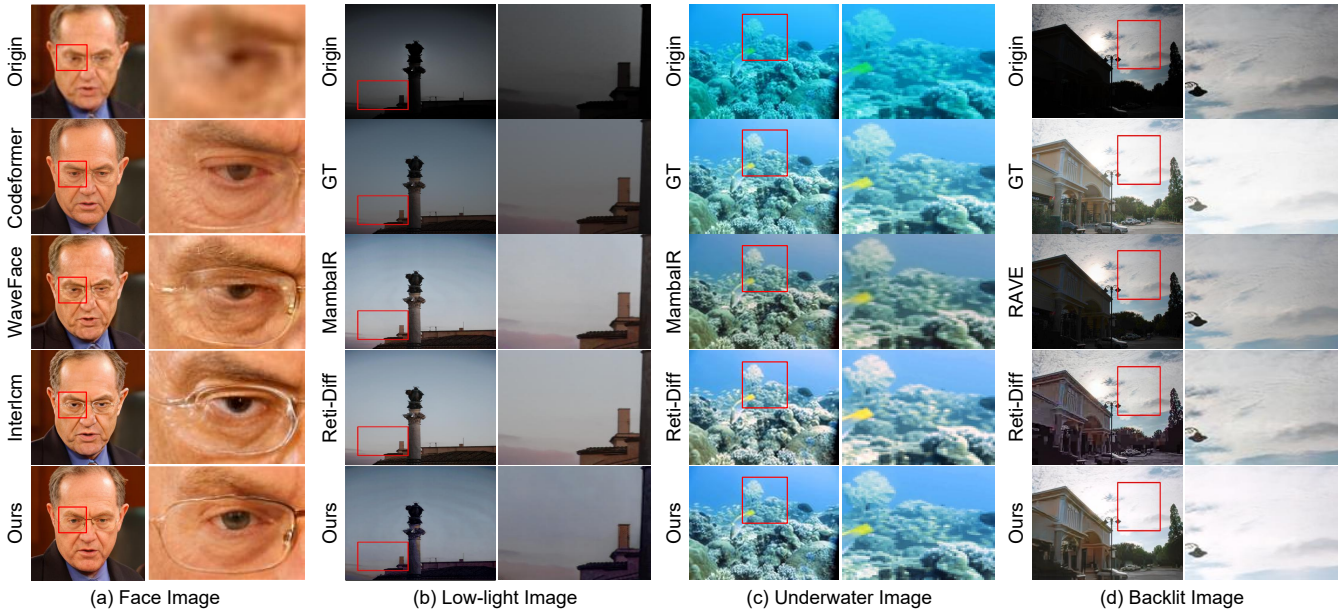


Figure 5. Visualizations on low light, underwater and backlit image restoration.

Table 3. Results on underwater image enhancement.

Methods	Sources	<i>UIEB</i>			
		PSNR $\uparrow$	SSIM $\uparrow$	UCIQE $\uparrow$	UIQM $\uparrow$
PUGAN [4]	TIP23	23.05	0.897	0.608	2.902
ADP [65]	IICV23	22.90	0.892	0.621	3.005
NU2Net [11]	AAAI23	22.38	0.903	0.587	2.936
AST [67]	CVPR24	22.19	0.908	0.602	2.981
MambaIR [12]	ECCV24	22.60	<b>0.916</b>	0.617	2.991
Reti-Diff [15]	ICLR25	<b>24.12</b>	0.910	<b>0.631</b>	<b>3.088</b>
IQPIR	Ours	<b>24.35</b>	<b>0.918</b>	<b>0.642</b>	<b>3.127</b>

Table 4. Results on backlit image enhancement.

Methods	Sources	<i>BAID</i>			
		PSNR $\uparrow$	SSIM $\uparrow$	LPIPS $\downarrow$	FID $\downarrow$
CLIP-LIT [32]	ICCV23	21.13	0.853	0.159	37.30
DiffIR [52]	ICCV23	21.10	0.835	0.175	40.35
AST [67]	CVPR24	22.61	0.851	0.156	32.47
MambaIR [12]	ECCV24	23.07	0.874	0.153	29.13
RAVE [8]	ECCV24	21.26	0.872	<b>0.096</b>	64.89
Reti-Diff [15]	ICLR25	<b>23.19</b>	<b>0.876</b>	0.147	<b>27.47</b>
IQPIR	Ours	<b>24.06</b>	<b>0.885</b>	<b>0.083</b>	<b>25.32</b>

aesthetic quality), Arniqa [1], MDFS [41], CLIP-IQA [46] and Q-Align [51]. Results in Tab. 1 show that IQPIR achieves superior performance across all datasets. Particularly, for Musiq-GFIQA and TOPIQ-GFIQA (metrics designed for evaluating face quality), IQPIR attains substantial improvements. Qualitative comparisons in Fig. 5 further demonstrate that IQPIR recovers finer facial details with more realistic textures and natural color tones.

**Low-light image enhancement.** Following the setting of Reti-Diff [15], we evaluate the performance on *LOL-v1* [50], *LOL-v2-real* [56], and *LOL-v2-synthetic* [56]. Four metrics are used for evaluation, including PSNR, SSIM, FID [21], and BIQE [40], where higher PSNR or SSIM, and

lower FID or BIQE correspond to better results. As depicted in Tab. 2, our IQPIR achieves a leading place across all metrics, indicating the superiority of our perception prior.

**Underwater image enhancement.** Following [15], we evaluate the performance on the *UIEB* [27] dataset. Two extra metrics, UCIQE [55] and UIQM [42], are used, where higher values mean better performance. As shown in Tab. 3 and Fig. 5, we achieve better performance qualitatively and quantitatively. This demonstrates that IQPIR effectively improves image quality under underwater conditions, outperforming competing methods in clarity and visual appeal.

**Backlit image enhancement.** Following [32], we evaluate the performance of our method on the *BAID* dataset using

Table 5. Break down ablation.

ID	Score Condition	Dual Codebook	Quality Optimization	TOPIQ-G $\uparrow$	Musiq-K $\uparrow$	Arniqa $\uparrow$	MDFS $\downarrow$	Q-Align $\uparrow$	CLIP-IQA $\uparrow$	Inference time (ms) $\downarrow$
(a)	×	×	×	0.757	73.53	0.675	20.03	3.78	0.742	5.27
(b)	✓	×	×	0.790	75.95	0.713	18.87	4.03	0.768	5.39
(c)	✓	✓	×	0.806	76.04	0.731	18.52	4.16	0.776	5.63
(d)	✓	✓	✓	<b>0.822</b>	<b>76.86</b>	<b>0.742</b>	18.30	<b>4.23</b>	0.783	5.63

Table 6. User study, where we conduct experiments on blind face restoration and low-light image enhancement.

(a) Blind Face Restoration					(b) Low-light Image Enhancement				
Methods	<i>LFW Test</i>	<i>WebPhoto Test</i>	<i>WIDER Test</i>	Mean	Methods	<i>LOL-v1</i>	<i>LOL-v2-real</i>	<i>LOL-v2-synthetic</i>	Mean
DiffFace [58]	2.50	2.58	2.08	2.39	AST [67]	3.08	3.42	3.58	3.36
DAEFR [45]	3.42	3.58	2.17	3.06	MambaIR [12]	3.67	3.58	3.16	3.47
WaveFace [38]	3.92	4.08	3.17	3.72	Reti-Diff [15]	4.42	3.50	3.67	3.86
Interlcm [28]	3.58	3.92	3.42	3.64	CIDNet [54]	3.50	3.25	3.59	3.45
IQPIR (Ours)	<b>4.17</b>	<b>4.25</b>	<b>3.67</b>	<b>4.03</b>	IQPIR (Ours)	<b>4.58</b>	<b>3.92</b>	<b>4.17</b>	<b>4.22</b>



Figure 6. Visualization of breakdown ablation, where (a), (b), (c), and (d) are consistent with those in Tab. 5.

PSNR, SSIM, LPIPS [62], and FID metrics. A lower LPIPS value indicates better perceptual quality. As shown in Tab. 4 and Fig. 5, our approach achieves leading results, demonstrating clear advantages in detail preservation and reduced color distortion compared to competing methods.

## 4.2. Ablation Study

We conduct experiments on *WebPhoto-Test*. For space limitations, only partial ablations are included; see supplementary materials for more details, such as the size of HQ+ Codebook, the fusion manners of quantized feature, and the incorporation manner of the perception prior.

**Quality Prior Conditional Approach.** We typically use the maximum score as the condition to achieve the best restoration quality. As shown in Tab. 5, (a) and (b) demonstrate the effectiveness of incorporating the quality prior into the codebook lookup Transformer. We further compare per-image runtime, showing that our approach achieves performance gains with only marginal computational overhead. The visualization in Fig. 6 also supports this—results from (b) produce sharper edges and richer textures compared to (a), validating the benefit of perception priors.

**Effectiveness of Dual Codebook.** The comparison between experiments (b) and (c) in Tab. 5 reveals that the proposed dual codebook consistently improves perceptual fidelity over the traditional single-codebook baseline. Fig. 6 further illustrates that (b) generates more distinct facial details than (c), confirming the capability of the HQ+ codebook to preserve high-quality features.

**Quality Optimization.** Ablations (c) and (d) in Tab. 5 high-



Figure 7. Quality in continuous (a) and discrete (b) representation space. Our discrete strategy shows score-quality consistency.

light the effectiveness of quality optimization. The discrete representation learned by the codebook enables the model to enhance reconstruction quality while avoiding the over-optimization issue often seen in continuous spaces. As depicted in Fig. 6, quality optimization further refines details and improves overall perceptual realism.

**Discrete Representation Mitigate Over-optimization.** As shown in Fig. 7, we compare quality optimization in continuous and discrete representation spaces. In the continuous space, results achieve high quality scores but exhibit poor perceptual realism. In contrast, the discrete representation space achieves both high scores and strong human-perceived quality, effectively mitigating over-optimization.

## 4.3. Further Analysis and Extended Applications

**User Study.** We conduct a user study on BFR (*LFW Test*, *WebPhoto Test*, and *WIDER Test*) and LLIE (*LOL-v1*, *LOL-v2-real*, and *LOL-v2-synthesize*) tasks. Twelve participants evaluated restored images on a 0–5 scale (0=worst,5=best) based on three criteria: color fidelity, noise/artifact suppression, and structural preservation. For fairness, each low-quality image and its restored one were displayed side by side, with method identities hidden. As shown in Tab. 6, our method consistently received the highest ratings, confirming its superiority in visual quality and perception.

**The Effect of Condition Score during Testing.** We show that the condition score directly influences restoration quality during testing. As illustrated in Fig. 9, adjusting the target score allows continuous control over perceptual quality. In practice, we typically use the maximum score to achieve

Table 7. Effect of our IQPIR (BFR).

Data.	Metrics	WavvFace	WaveFace+	InterIcm	InterIcm+
<i>LFW-Test</i>	Topiq-G $\uparrow$	0.786	0.802	0.831	0.850
	Musiq-G $\uparrow$	0.799	0.817	0.834	0.852
	Q-Align $\uparrow$	4.43	4.53	4.55	4.67
	CLIP-IQA $\uparrow$	0.788	0.793	0.721	0.737
	Gain	—	1.8 %	—	2.33%
<i>WIDER-Test</i>	Topiq-G $\uparrow$	0.751	0.775	0.798	0.813
	Musiq-G $\uparrow$	0.778	0.808	0.820	0.844
	Q-Align $\uparrow$	4.12	4.35	4.24	4.38
	CLIP-IQA $\uparrow$	0.781	0.792	0.754	0.765
	Gain	—	3.54 %	—	2.39%

Table 8. Effect of our IQPIR (LLIE).

Data.	Metrics	Reti-Diff	Reti-Diff+	CIDNet	CIDNet+
<i>LOL-v1</i>	PSNR $\uparrow$	25.35	25.52	23.50	24.28
	SSIM $\uparrow$	0.866	0.889	0.900	0.908
	FID $\downarrow$	49.14	42.15	46.69	40.36
	BIQE $\downarrow$	17.75	15.35	14.77	13.73
	Gain	—	7.77 %	—	6.20%
<i>LOL-v2-real</i>	PSNR $\uparrow$	22.97	23.73	24.11	24.73
	SSIM $\uparrow$	0.858	0.868	0.871	0.882
	FID $\downarrow$	43.18	40.15	48.04	43.33
	BIQE $\downarrow$	23.66	19.57	18.45	16.31
	Gain	—	7.19 %	—	5.94%

Table 9. Effect of our IQPIR (UIE and BIE).

Data.	Metrics	MambaIR	MambaIR+	Reti-Diff	Reti-Diff+
<i>UIEB</i>	PSNR $\uparrow$	22.60	23.72	24.12	24.28
	SSIM $\uparrow$	0.914	0.920	0.911	0.917
	UCIQE $\uparrow$	0.617	0.632	0.630	0.638
	UIQM $\uparrow$	2.991	3.208	3.087	3.219
	Gain	—	3.77 %	—	1.69%
<i>BAMD</i>	PSNR $\uparrow$	23.07	23.62	23.19	23.83
	SSIM $\uparrow$	0.874	0.877	0.876	0.880
	LPIPS $\downarrow$	0.153	0.137	0.146	0.125
	FID $\downarrow$	29.13	27.85	27.47	24.76
	Gain	—	4.37 %	—	7.04%

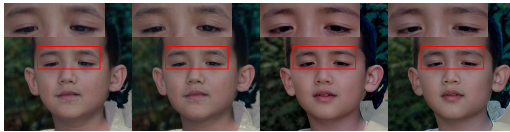


Figure 8. Generalization of our IQPIR.

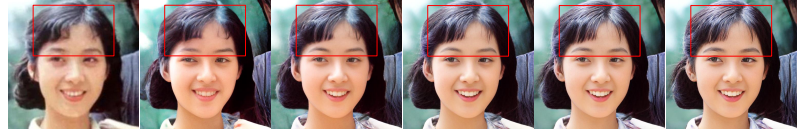


Figure 9. Visualization with different condition scores.

Table 10. Low-light image detection on *ExDark*.

Methods (AP)	Bicycle	Boat	Bottle	Bus	Car	Cat	Chair	Cup	Dog	Motor	People	Table	Mean
Baseline	74.7	64.9	70.7	84.2	79.7	47.3	58.6	67.1	64.1	66.2	73.9	45.7	66.4
MIRNet [60]	74.9	69.7	68.3	89.7	77.6	57.8	56.9	66.4	69.7	64.6	74.6	53.4	68.6
RUAS [34]	75.7	71.2	73.5	90.7	80.1	59.3	67.0	66.3	68.3	66.9	72.6	50.6	70.2
Restormer [61]	77.0	71.0	68.8	91.6	77.1	62.5	57.3	68.0	69.6	69.2	74.6	49.7	69.7
SCI [37]	73.4	68.0	69.5	86.2	74.5	63.1	59.5	61.0	67.3	63.9	73.2	47.3	67.2
SNR-Net [53]	78.3	74.2	74.5	89.6	82.7	66.8	66.3	62.5	74.7	63.1	73.3	57.2	71.9
Reti-Diff [15]	82.0	77.9	76.4	92.2	83.3	69.6	67.4	74.4	75.5	74.3	<b>78.3</b>	57.9	75.8
CIDNet [54]	81.8	77.6	77.2	85.8	77.3	68.1	65.5	73.6	74.7	70.2	71.0	60.3	73.6
Reti-Diff+	82.5	<b>78.3</b>	<b>77.2</b>	<b>92.7</b>	<b>83.7</b>	<b>70.5</b>	<b>69.6</b>	<b>76.3</b>	<b>77.2</b>	<b>76.1</b>	<b>79.7</b>	60.2	<b>77.0</b>
CIDNet+	<b>82.7</b>	78.2	<b>77.6</b>	87.6	77.9	69.700	67.3	75.9	<b>77.3</b>	73.8	72.5	<b>63.7</b>	75.4
IQPIR	<b>83.4</b>	<b>80.2</b>	<b>77.5</b>	<b>92.5</b>	<b>83.6</b>	<b>75.7</b>	<b>77.8</b>	<b>78.4</b>	<b>79.3</b>	<b>82.5</b>	77.3	<b>65.3</b>	<b>79.5</b>

the best restoration results. Although quality controllability may seem less essential for BFR, its main purpose is to ensure the model reaches the highest-quality output rather than to serve as an independent control mechanism.

**Generalizability of IQPIR.** We further evaluate the generalization capability of IQPIR by integrating the proposed perception prior into several SOTA restoration methods across diverse tasks. For comprehensive evaluation, four specific metrics are employed for each task. As shown in Tabs. 7 to 9, IQPIR consistently enhances the performance of six representative models on their benchmarks, confirming the versatility and robustness of our framework. To further verify this, we add a visualization in Fig. 8, where the method integrated with our framework shows more detailed texture information and more harmonious visual fidelity.

**Color Enhancement.** We compare IQPIR with CodeFormer [66] and CodeFormer+, where CodeFormer+ denotes CodeFormer enhanced with our perception prior. IQPIR produces results with more natural color rendition and richer facial details than competing methods. Moreover, CodeFormer+ yields more visually balanced and realistic color tones compared to the original CodeFormer. This indicates that our IQPIR is a plug-and-play image prior with strong generalization capacity.

**Benefits for downstream tasks.** Improving image quality can facilitate various downstream vision tasks. To verify this, we assess the impact of enhancement on low-light ob-

ject detection. Specifically, low-quality images from ExDark [35] are enhanced using different algorithms and subsequently fed into YOLO for detection. For reference, we also include a baseline that directly uses the original low-quality inputs without enhancement. As reported in Tab. 10, IQPIR achieves the highest detection performance and further provides consistent performance gains when integrated into other restoration frameworks.

## 5. Limitations and Future Works

The quality priors employed by our IQPIR are directly derived from existing NR-IQA models. Although this design simplifies implementation and enables effective perceptual guidance, it may also inherit biases intrinsic to the IQA models, which can lead to potential inaccuracies in quality estimation. In future work, we plan to address this limitation by exploring more principled approaches to integrate quality priors with restoration models. In particular, we will investigate strategies to mitigate the influence of biases introduced by individual IQA models, such as adopting adaptive ensemble schemes or jointly optimizing the IQA priors together with the restoration objectives.

## 6. Conclusions

We presented IQPIR, a perception-driven framework for RWIR that integrates IQP with discrete codebook repre-

sentations. By leveraging NR-IQA-based priors and a dual-codebook architecture, IQPIR guides the restoration process toward perceptually optimal results while preserving structural fidelity. Our quality-conditioned transformer further enhances adaptation to diverse degradation types. Experiments demonstrate that IQPIR achieves SOTA performance and offers a generalizable paradigm that can be readily integrated into existing restoration frameworks.

## References

- [1] Lorenzo Agnolucci, Leonardo Galteri, Marco Bertini, and Alberto Del Bimbo. Arniqa: Learning distortion manifold for image quality assessment. In *Proceedings of the IEEE/CVF Winter Conference on Applications of Computer Vision*, pages 189–198, 2024. 6
- [2] Chaofeng Chen, Xiaoming Li, Lingbo Yang, Xianhui Lin, Lei Zhang, and Kwan-Yee K Wong. Progressive semantic-aware style transformation for blind face restoration. In *Proceedings of the IEEE/CVF conference on computer vision and pattern recognition*, pages 11896–11905, 2021. 3
- [3] Chaofeng Chen, Jiadi Mo, Jingwen Hou, Haoning Wu, Liang Liao, Wenxiu Sun, Qiong Yan, and Weisi Lin. Topiq: A top-down approach from semantics to distortions for image quality assessment. *IEEE Transactions on Image Processing*, 2024. 5
- [4] Runmin Cong, Wenyu Yang, Wei Zhang, Chongyi Li, Chunle Guo, Qingming Huang, and Sam Kwong. Pugan: Physical model-guided underwater image enhancement using gan with dual-discriminators. *IEEE Transactions on Image Processing*, 2023. 6
- [5] Lizhen Deng, Chunming He, Guoxia Xu, Hu Zhu, and Hao Wang. Pcgan: A noise robust conditional generative adversarial network for one shot learning. *IEEE transactions on intelligent transportation systems*, 23(12):25249–25258, 2022. 3
- [6] Patrick Esser, Robin Rombach, and Bjorn Ommer. Taming transformers for high-resolution image synthesis. In *Proceedings of the IEEE/CVF conference on computer vision and pattern recognition*, pages 12873–12883, 2021. 3
- [7] Chengyu Fang, Chunming He, Fengyang Xiao, Yulun Zhang, Longxiang Tang, Yuelin Zhang, Kai Li, and Xiu Li. Real-world image dehazing with coherence-based label generator and cooperative unfolding network. *NeurIPS*, pages arXiv–2406, 2024. 3
- [8] Tatiana Gaintseva, Martin Benning, and Gregory Slabaugh. Rave: Residual vector embedding for clip-guided backlit image enhancement. In *ECCV*, pages 412–428. Springer, 2024. 6
- [9] Leo Gao, John Schulman, and Jacob Hilton. Scaling laws for reward model overoptimization. In *International Conference on Machine Learning*, pages 10835–10866. PMLR, 2023. 4
- [10] Yuchao Gu, Xintao Wang, Liangbin Xie, Chao Dong, Gen Li, Ying Shan, and Ming-Ming Cheng. Vqfr: Blind face restoration with vector-quantized dictionary and parallel decoder. In *European Conference on Computer Vision*, pages 126–143. Springer, 2022. 1, 3
- [11] Chunle Guo, Ruiqi Wu, Xin Jin, Linghao Han, Weidong Zhang, Zhi Chai, and Chongyi Li. Underwater ranker: Learn which is better and how to be better. In *Proceedings of the AAAI conference on artificial intelligence*, pages 702–709, 2023. 6
- [12] Hang Guo, Jinmin Li, Tao Dai, Zhihao Ouyang, Xudong Ren, and Shu-Tao Xia. Mambair: A simple baseline for image restoration with state-space model. In *ECCV*, 2024. 6, 7
- [13] Chunming He, Kai Li, Guoxia Xu, Jiangpeng Yan, Longxiang Tang, Yulun Zhang, Yaowei Wang, and Xiu Li. Hqgnnet: Unpaired medical image enhancement with high-quality guidance. *TNNLS*, 2023. 3
- [14] Chunming He, Kai Li, and Yulun Zhang. Degradation-resistant unfolding network for heterogeneous image fusion. In *ICCV*, pages 611–621, 2023. 3
- [15] Chunming He, Chengyu Fang, Yulun Zhang, Kai Li, Longxiang Tang, Chenyu You, Fengyang Xiao, Zhenhua Guo, and Xiu Li. Reti-diff: Illumination degradation image restoration with retinex-based latent diffusion model. *ICLR*, 2025. 3, 6, 7, 8
- [16] Chunming He, Kai Li, Yachao Zhang, Ziyun Yang, Longxiang Tang, Yulun Zhang, Linghe Kong, and Sina Farsiu. Segment concealed object with incomplete supervision. *IEEE Trans. Pattern Anal. Mach. Intell.*, 2025. 3
- [17] Chunming He, Fengyang Xiao, Rihan Zhang, Chengyu Fang, Deng-Ping Fan, and Sina Farsiu. Reversible unfolding network for concealed visual perception with generative refinement. *arXiv preprint arXiv:2508.15027*, 2025. 3
- [18] Chunming He, Rihan Zhang, Fengyang Xiao, Chengyu Fang, Longxiang Tang, Yulun Zhang, and Sina Farsiu. Unfoldir: Rethinking deep unfolding network in illumination degradation image restoration. *arXiv preprint arXiv:2505.06683*, 2025. 3
- [19] Chunming He, Rihan Zhang, Fengyang Xiao, Chenyu Fang, Longxiang Tang, Yulun Zhang, Linghe Kong, Deng-Ping Fan, Kai Li, and Sina Farsiu. Run: Reversible unfolding network for concealed object segmentation. *ICML*, 2025. 3
- [20] Jingwen He, Wu Shi, Kai Chen, Lean Fu, and Chao Dong. Gcfsr: a generative and controllable face super resolution method without facial and gan priors. In *Proceedings of the IEEE/CVF Conference on Computer Vision and Pattern Recognition*, pages 1889–1898, 2022. 3
- [21] Martin Heusel, Hubert Ramsauer, Thomas Unterthiner, Bernhard Nessler, and Sepp Hochreiter. Gans trained by a two time-scale update rule converge to a local nash equilibrium. *Advances in neural information processing systems*, 30, 2017. 6
- [22] Xiaobin Hu, Wenqi Ren, Jiaolong Yang, Xiaoqun Cao, David Wipf, Bjoern Menze, Xin Tong, and Hongbin Zha. Face restoration via plug-and-play 3d facial priors. *IEEE Transactions on Pattern Analysis and Machine Intelligence*, 44(12):8910–8926, 2021. 3
- [23] Gary B Huang, Marwan Mattar, Tamara Berg, and Eric Learned-Miller. Labeled faces in the wild: A database for studying face recognition in unconstrained environments. In *Workshop on faces in 'Real-Life' Images: detection, alignment, and recognition*, 2008. 5

- [24] HOU Jinhui, Zhiyu Zhu, Junhui Hou, LIU Hui, Huanqiang Zeng, and Hui Yuan. Global structure-aware diffusion process for low-light image enhancement. In *NeurIPS*, 2023. 6
- [25] Tero Karras, Samuli Laine, and Timo Aila. A style-based generator architecture for generative adversarial networks. In *Proceedings of the IEEE/CVF conference on computer vision and pattern recognition*, pages 4401–4410, 2019. 3
- [26] Junjie Ke, Qifei Wang, Yilin Wang, Peyman Milanfar, and Feng Yang. Musiq: Multi-scale image quality transformer. In *Proceedings of the IEEE/CVF International Conference on Computer Vision*, pages 5148–5157, 2021. 5
- [27] Chongyi Li, Chunle Guo, Wenqi Ren, Runmin Cong, Junhui Hou, Sam Kwong, and Dacheng Tao. An underwater image enhancement benchmark dataset and beyond. *IEEE Transactions on Image Processing*, 29:4376–4389, 2019. 6
- [28] Senmao Li, Kai Wang, Joost van de Weijer, Fahad Shahbaz Khan, Chun-Le Guo, Shiqi Yang, Yaxing Wang, Jian Yang, and Ming-Ming Cheng. Interlcm: Low-quality images as intermediate states of latent consistency models for effective blind face restoration. *ICLR*, 2025. 3, 5, 7
- [29] Xiaoming Li, Ming Liu, Yuting Ye, Wangmeng Zuo, Liang Lin, and Ruigang Yang. Learning warped guidance for blind face restoration. In *Proceedings of the European conference on computer vision (ECCV)*, pages 272–289, 2018. 3
- [30] Xiaoming Li, Chaofeng Chen, Shangchen Zhou, Xianhui Lin, Wangmeng Zuo, and Lei Zhang. Blind face restoration via deep multi-scale component dictionaries. In *European conference on computer vision*, pages 399–415. Springer, 2020. 1, 3
- [31] Xiaoming Li, Wenyu Li, Dongwei Ren, Hongzhi Zhang, Meng Wang, and Wangmeng Zuo. Enhanced blind face restoration with multi-exemplar images and adaptive spatial feature fusion. In *Proceedings of the IEEE/CVF Conference on Computer Vision and Pattern Recognition*, pages 2706–2715, 2020. 1, 3
- [32] Zhexin Liang, Chongyi Li, Shangchen Zhou, Ruicheng Feng, and Chen Change Loy. Iterative prompt learning for unsupervised backlit image enhancement. In *ICCV*, pages 8094–8103, 2023. 6
- [33] Xinqi Lin, Jingwen He, Ziyang Chen, Zhaoyang Lyu, Bo Dai, Fanghua Yu, Yu Qiao, Wanli Ouyang, and Chao Dong. Diffbir: Toward blind image restoration with generative diffusion prior. In *European Conference on Computer Vision*, pages 430–448. Springer, 2024. 3
- [34] Risheng Liu, Long Ma, Jiaao Zhang, Xin Fan, and Zhongxuan Luo. Retinex-inspired unrolling with cooperative prior architecture search for low-light image enhancement. In *CVPR*, pages 10561–10570, 2021. 8
- [35] Yuen Peng Loh and Chee Seng Chan. Getting to know low-light images with the exclusively dark dataset. *Computer Vision and Image Understanding*, 178:30–42, 2019. 8
- [36] Cheng Ma, Zhenyu Jiang, Yongming Rao, Jiwen Lu, and Jie Zhou. Deep face super-resolution with iterative collaboration between attentive recovery and landmark estimation. In *Proceedings of the IEEE/CVF conference on computer vision and pattern recognition*, pages 5569–5578, 2020. 1, 3
- [37] Long Ma, Tengyu Ma, Risheng Liu, Xin Fan, and Zhongxuan Luo. Toward fast, flexible, and robust low-light image enhancement. In *CVPR*, pages 5637–5646, 2022. 8
- [38] Yunqi Miao, Jiankang Deng, and Jungong Han. Waveface: Authentic face restoration with efficient frequency recovery. In *Proceedings of the IEEE/CVF Conference on Computer Vision and Pattern Recognition*, pages 6583–6592, 2024. 5, 7
- [39] Anish Mittal, Anush Krishna Moorthy, and Alan Conrad Bovik. No-reference image quality assessment in the spatial domain. *IEEE Transactions on image processing*, 21(12):4695–4708, 2012. 5
- [40] Anush Krishna Moorthy and Alan Conrad Bovik. A two-step framework for constructing blind image quality indices. *IEEE Signal processing letters*, 17(5):513–516, 2010. 6
- [41] Zhangkai Ni, Yue Liu, Keyan Ding, Wenhan Yang, Hanli Wang, and Shiqi Wang. Opinion-unaware blind image quality assessment using multi-scale deep feature statistics. *IEEE Transactions on Multimedia*, 2024. 6
- [42] Karen Panetta, Chen Gao, and Sos Agaian. Human-visual-system-inspired underwater image quality measures. *IEEE Journal of Oceanic Engineering*, 41(3):541–551, 2015. 6
- [43] Guanyi Qin, Runze Hu, Yutao Liu, Xiawu Zheng, Haotian Liu, Xiu Li, and Yan Zhang. Data-efficient image quality assessment with attention-panel decoder. In *AAAI*, pages 2091–2100, 2023. 3
- [44] Shaolin Su, Hanhe Lin, Vlad Hosu, Oliver Wiedemann, Jinqiu Sun, Yu Zhu, Hantao Liu, Yanning Zhang, and Dietmar Saupe. Going the extra mile in face image quality assessment: A novel database and model. *IEEE Transactions on Multimedia*, 2023. 5
- [45] Yu-Ju Tsai, Yu-Lun Liu, Lu Qi, Kelvin CK Chan, and Ming-Hsuan Yang. Dual associated encoder for face restoration. *ICLR*, 2024. 1, 3, 5, 7
- [46] Jianyi Wang, Kelvin CK Chan, and Chen Change Loy. Exploring clip for assessing the look and feel of images. In *Proceedings of the AAAI Conference on Artificial Intelligence*, pages 2555–2563, 2023. 5, 6
- [47] Xintao Wang, Yu Li, Honglun Zhang, and Ying Shan. Towards real-world blind face restoration with generative facial prior. In *The IEEE Conference on Computer Vision and Pattern Recognition (CVPR)*, 2021. 1, 3, 5
- [48] Zhouxia Wang, Jiawei Zhang, Runjian Chen, Wenping Wang, and Ping Luo. Restoreformer: High-quality blind face restoration from undegraded key-value pairs. In *Proceedings of the IEEE/CVF Conference on Computer Vision and Pattern Recognition*, pages 17512–17521, 2022. 1, 5
- [49] Zhixin Wang, Ziyang Zhang, Xiaoyun Zhang, Huangjie Zheng, Mingyuan Zhou, Ya Zhang, and Yanfeng Wang. Dr2: Diffusion-based robust degradation remover for blind face restoration. In *Proceedings of the IEEE/CVF Conference on Computer Vision and Pattern Recognition*, pages 1704–1713, 2023. 1, 3, 5
- [50] Chen Wei, Wenjing Wang, Wenhan Yang, and Jiaying Liu. Deep retinex decomposition for low-light enhancement. *arXiv preprint arXiv:1808.04560*, 2018. 6
- [51] Haoning Wu, Zicheng Zhang, Weixia Zhang, Chaofeng Chen, Liang Liao, Chunyi Li, Yixuan Gao, Annan Wang,

- Erli Zhang, Wenxiu Sun, et al. Q-align: Teaching Imms for visual scoring via discrete text-defined levels. *ICLR*, 2024. [5](#), [6](#)
- [52] Bin Xia, Yulun Zhang, Shiyin Wang, Yitong Wang, Xinglong Wu, Yapeng Tian, Wenming Yang, and Luc Van Gool. Diffir: Efficient diffusion model for image restoration. In *ICCV*, 2023. [6](#)
- [53] Xiaogang Xu, Ruixing Wang, Chi-Wing Fu, and Jiaya Jia. Snr-aware low-light image enhancement. In *CVPR*, pages 17714–17724, 2022. [8](#)
- [54] Qingsen Yan, Yixu Feng, Cheng Zhang, Pei Wang, Peng Wu, Wei Dong, Jinqu Sun, and Yanning Zhang. You only need one color space: An efficient network for low-light image enhancement. *CVPR*, 2025. [6](#), [7](#), [8](#)
- [55] Miao Yang and Arcot Sowmya. An underwater color image quality evaluation metric. *IEEE Transactions on Image Processing*, 24(12):6062–6071, 2015. [6](#)
- [56] Wenhao Yang, Wenjing Wang, Haofeng Huang, Shiqi Wang, and Jiaying Liu. Sparse gradient regularized deep retinex network for robust low-light image enhancement. *IEEE Transactions on Image Processing*, 30:2072–2086, 2021. [6](#)
- [57] Fanghua Yu, Jinjin Gu, Zheyuan Li, Jinfan Hu, Xiangtao Kong, Xintao Wang, Jingwen He, Yu Qiao, and Chao Dong. Scaling up to excellence: Practicing model scaling for photo-realistic image restoration in the wild. In *CVPR*, pages 25669–25680, 2024. [3](#)
- [58] Zongsheng Yue and Chen Change Loy. Difface: Blind face restoration with diffused error contraction. *IEEE Transactions on Pattern Analysis and Machine Intelligence*, 2024. [2](#), [5](#), [7](#)
- [59] Zongsheng Yue, Qian Zhao, Lei Zhang, and Deyu Meng. Dual adversarial network: Toward real-world noise removal and noise generation. In *ECCV*, pages 41–58, 2020. [3](#)
- [60] Syed Waqas Zamir, Aditya Arora, Salman Khan, Munawar Hayat, Fahad Shahbaz Khan, Ming-Hsuan Yang, and Ling Shao. Learning enriched features for real image restoration and enhancement. In *ECCV*, pages 492–511. Springer, 2020. [8](#)
- [61] Syed Waqas Zamir, Aditya Arora, Salman Khan, Munawar Hayat, Fahad Shahbaz Khan, and Ming-Hsuan Yang. Restormer: Efficient transformer for high-resolution image restoration. In *CVPR*, pages 5728–5739, 2022. [8](#)
- [62] Richard Zhang, Phillip Isola, Alexei A Efros, Eli Shechtman, and Oliver Wang. The unreasonable effectiveness of deep features as a perceptual metric. In *Proceedings of the IEEE conference on computer vision and pattern recognition*, pages 586–595, 2018. [7](#)
- [63] Yang Zhao, Tingbo Hou, Yu-Chuan Su, Xuhui Jia Li, Matthias Grundmann, et al. Towards authentic face restoration with iterative diffusion models and beyond. *ICCV*, 2023. [1](#), [3](#)
- [64] Naishan Zheng, Man Zhou, Yanmeng Dong, Xiangyu Rui, Jie Huang, Chongyi Li, and Feng Zhao. Empowering low-light image enhancer through customized learnable priors. In *ICCV*, pages 12559–12569, 2023. [6](#)
- [65] Jingchun Zhou, Qian Liu, Qiuping Jiang, Wenqi Ren, Kin-Man Lam, and Weishi Zhang. Underwater camera: Improving visual perception via adaptive dark pixel prior and color correction. *International Journal of Computer Vision*, pages 1–19, 2023. [6](#)
- [66] Shangchen Zhou, Kelvin Chan, Chongyi Li, and Chen Change Loy. Towards robust blind face restoration with codebook lookup transformer. *Advances in Neural Information Processing Systems*, 35:30599–30611, 2022. [1](#), [3](#), [5](#), [8](#)
- [67] Shihao Zhou, Duosheng Chen, Jinshan Pan, Jinglei Shi, and Jufeng Yang. Adapt or perish: Adaptive sparse transformer with attentive feature refinement for image restoration. In *CVPR*, pages 2952–2963, 2024. [6](#), [7](#)